Design and Simulation of Thermo‐Responsive 4D Hydrogel Materials

Jee, Chanhyuk
Department of Chemical Engineering, Graduate School of Engineering, Kyushu University

Matsumoto, Hikaru
Department of Chemical Engineering, Graduate School of Engineering, Kyushu University

Liu, Zaiyang
Department of Robotics, Ritsumeikan University

Wang, Zhongkui
Department of Robotics, Ritsumeikan University

他

出版情報：Journal of Polymer Science. 63 (19), pp.3882-3891, 2025-07-13. Wiley
バージョン：

Journal of Polymer Science

WILEY

JOURNAL OF POLYMER SCIENCE

RESEARCH ARTICLE OPEN ACCESS

Design and Simulation of Thermo-Responsive 4D Hydrogel Materials

Chanhyuk Jee[1] | Hikaru Matsumoto[1] | Zaiyang Liu[2] | Zhongkui Wang[2] | Obayashi Kakeru[3] | Ken Kojio[4] | Mina Shigeyama[1] | Masanori Nagao[1] | Yoshiko Miura[1]

[1]Department of Chemical Engineering, Graduate School of Engineering, Kyushu University, Fukuoka, Japan | [2]Department of Robotics, Ritsumeikan University, Kusatsu, Japan | [3]Department of Applied Chemistry, Graduate School of Engineering, Kyushu University, Fukuoka, Japan | [4]Institute for Materials Chemistry and Engineering, Kyushu University, Fukuoka, Japan

Correspondence: Yoshiko Miura (miuray@chem-eng.kyushu-u.ac.jp)

Received: 12 April 2025 | **Revised:** 5 June 2025 | **Accepted:** 19 June 2025

Funding: This work was supported by New Energy and Industrial Technology Development Organization (NEDO), JPNP14004.

Keywords: 4D material | computer simulator | PET-RAFT | soft hydrogel material | thermo-responsive

ABSTRACT

Stimuli-responsive hydrogel materials have significantly contributed to advancements in various industries and the research field of smart actuators. By integrating computer simulations with 4D materials research, we have improved the precision of our studies and reduced research time. The fabrication of bilayer-designed stimuli-responsive hydrogels has been extensively investigated. In this study, we developed and analyzed bilayer-designed hydrogels using acrylamide (AM), *N*-isopropylacrylamide (NIPAm), and 3-[[2-(methacryloyloxy)ethyl]dimethylammonio]propane-1-sulfonate (SBMA) monomers. These hydrogels were based on LCST, UCST, and standard hydrogel formulations and were characterized using FT-IR spectroscopy, rheological measurements, and 4D motion analysis. The bilayer hydrogel samples, composed of LCST and UCST polymer materials (NIPAm and SBMA), demonstrated curvature and inverse-curvature 4D movements across a temperature range of 4°C70°C. By employing computer simulations to predict 4D movements in bilayer-designed samples, we achieved more precise insights into the properties of thermo-responsive hydrogel materials. This study highlights the potential of combining computer simulations with experimental approaches to design more complex and sophisticated 4D materials in the future.

1 | Introduction

Hydrogels, highly versatile and stimuli-responsive polymer networks, have become a cornerstone in the advancement of soft robotics [1, 2] and bio- [3, 4] and industry- [5] inspired applications. Their ability to retain significant amounts of water, exhibit flexibility, and respond dynamically to external stimuli such as temperature [6–11], pH [12, 13], and light [14, 15] uniquely positions them to mimic biological tissues [16, 17]. This adaptability makes them a key material for the design of 4D materials—advanced systems that change shape, structure, or function over time in response to environmental triggers. These attributes, combined with advancements in fabrication technologies, position hydrogels as an indispensable component of next-generation smart materials.

Recent developments in hydrogel science have emphasized the potential of bilayer structures, which integrate two distinct layers with opposing thermoresponsive properties, such as lower critical solution temperature (LCST) and upper critical solution temperature (UCST) [18–22]. These are known as Janus hydrogels [23, 24]. This combination enables hydrogels to perform complex actuations through controlled swelling and deswelling. For example, bilayer hydrogel actuators inspired by the Mimosa plant exhibit reverse thermal responsiveness [25], redistributing internal water between layers to

achieve bending motions. This innovation allows such actuators to function effectively not only in aqueous environments but also in non-aqueous and open-air conditions, greatly expanding their applicability in fields like robotics, microfluidics [26], and environmental sensing [27, 28].

Additionally, UCST-responsive hydrogels, such as those composed of poly(acrylamide-acrylic acid) copolymers, offer unique swelling and deswelling behaviors based on hydrogen bonding [27, 28]. These materials demonstrate the ability to undergo phase transitions, enabling precise control of structural and mechanical properties. This characteristic has significant implications for designing responsive soft actuators and devices tailored to specific environmental conditions, such as controlled drug delivery and adaptive interfaces [21, 24, 29–33].

Advances in 3D printing technologies have further transformed the potential of hydrogel systems, enabling the creation of complex bilayer structures with programmable and reversible shape-morphing capabilities. Using precise layered fabrication, hydrogels can be designed to exhibit highly controlled mechanical and thermal properties, optimizing their performance for specific tasks. For example, hydrogels combining LCST, UCST, and non-responsive layers, such as poly(*N*-isopropylacrylamide) (PNIPAm), poly[3-[[2-(methacryloyloxy)ethyl]dimethylammonio] propane-1-sulfonate] (poly(SBMA)), and poly(2-hydroxyethyl methacrylate) (poly(HEMA)), allow for shape transitions between flat and three-dimensional forms depending on hydration and temperature [19, 34, 35]. These programmable behaviors exemplify the utility of hydrogels as robust 4D materials, capable of integrating into dynamic systems like soft robotics, biomedical devices, and environmental sensors [36, 37].

This study seeks to build on these advancements by synthesizing Photoinduced Electron/Energy Transfer Reversible Addition-Fragmentation Chain-Transfer (PET-RAFT) hydrogels with tailored LCST and UCST properties and implementing them in bilayer architectures (Figure 1) [38, 39]. By integrating the principles of 4D materials with the structural and functional advantages of bilayer hydrogels, this work aims to expand the capabilities of soft actuators in diverse and challenging environments. Through the combination of advanced polymerization techniques and bio-inspired designs, this research contributes to the growing field of smart materials, laying the groundwork for innovative applications in robotics, healthcare, and adaptive technologies. Furthermore, computational simulator technologies are widely used in the research of 4D materials. These include computational design [36] for various purposes and property expectations, and mathematical modeling technologies for 4D movement [40].

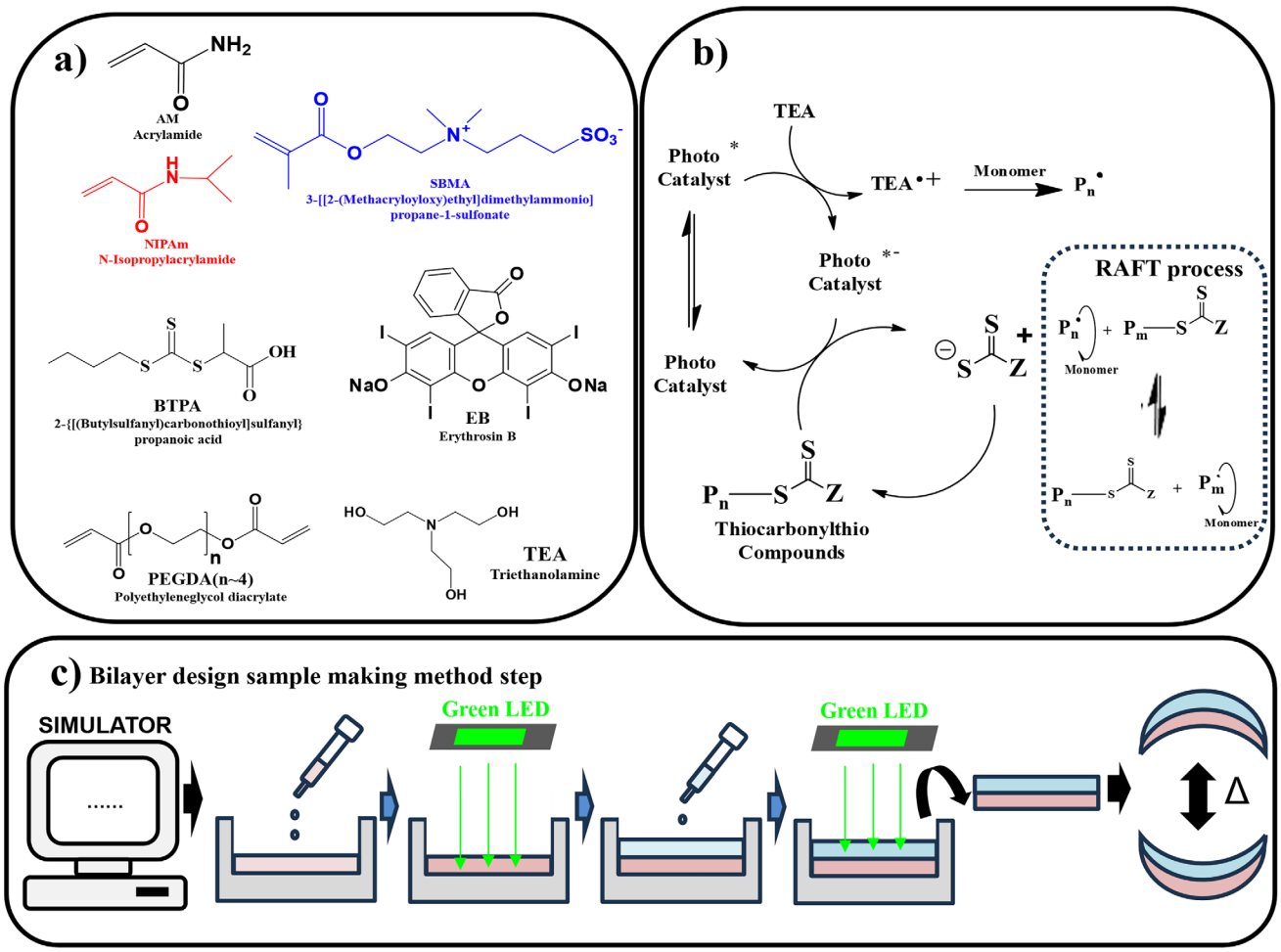

FIGURE 1 | Preparation of hydrogels by PET-RAFT polymerization. (a) Chemical structures of monomers and PET-RAFT reagents, (b) mechanism of PET-RAFT polymerization, and (c) preparation of hydrogels for 4D materials with bilayer structure.

2 | Experimental

2.1 | Materials

Acrylamide (AM, 98.0%) and 3-[[2-(methacryloyloxy)ethyl] dimethylammonio]-propane-1-sulfonate (SBMA, 98.0%) were purchased from Tokyo Chemical Industry (TCI Co. Ltd., Tokyo, Japan). Polyethylene glycol diacrylate (PEGDA, $n \sim 4$) was purchased from TCI Co. Ltd. Triethanolamine (TEA, 98.0%) was purchased from Merck-Aldrich (Darmstadt, Germany). Erythrosin B (EB) was purchased from TCI Co. Ltd. 2{[(Butylsulfanyl) carbonothioyl] sulfanyl} propanoic acid (BTPA) was synthesized according to the previous report (Figure S1) [41]. *N*-Isopropylacrylamide (NIPAm) was purchased from FUJIFILM Wako Chemicals (Osaka, Japan) and purified by recrystallization using hexane.

2.2 | Preparation of Hydrogels by PET-RAFT Polymerization

The gel precursor for **1** (AM100 hydrogel) was prepared by dissolution of AM (5285 mM), PEGDA ($n \sim 4$, 27 mM), BTPA (5 mM), EB (0.3 mM), and TEA (106 mM) in water as matrix monomer, cross-linker, RAFT agent, photocatalyst, and reductant, respectively. The monomer mixer for **2** (AM25-NIPAm75 hydrogel) was prepared by dissolution of AM (917 mM) and NIPAm (2807 mM), PEGDA ($n \sim 4$, 19 mM), BTPA (4 mM), EB (0.19 mM), and TEA (75 mM) in water. The monomer mixer for **3** (AM50-SBMA50 hydrogel) was prepared by dissolution of AM (1103 mM), SBMA (1115 mM), PEGDA ($n \sim 4$, 11 mM), BTPA (11 mM), EB (0.5 mM), and TEA (212 mM) in water. The monomer mixer was poured into molds with round shape (200 μL/ea), which were maintained at controlled temperature (25°C) and humidity. For the preparation of **1** and **2**, the mold was irradiated with green light (518 nm) for 3 min. For the preparation of **3**, the mold was irradiated with the green light for 30 min (Scheme 1) (Figure S2).

2.3 | Characterization of the Prepared PET-RAFT Hydrogel Samples

2.3.1 | Attenuated Total Reflectance Fourier-Transform Infrared (ATR-FT IR) Spectroscopy

ATR-FT IR spectroscopy was performed to monitor using FT-IR-4700 (Jasco, Japan) spectrometer with ATR ZnSe crystal lens plate. A transmittance spectrum was obtained by scanning the droplet of the sample from 400 to 4000 cm^{-1}.

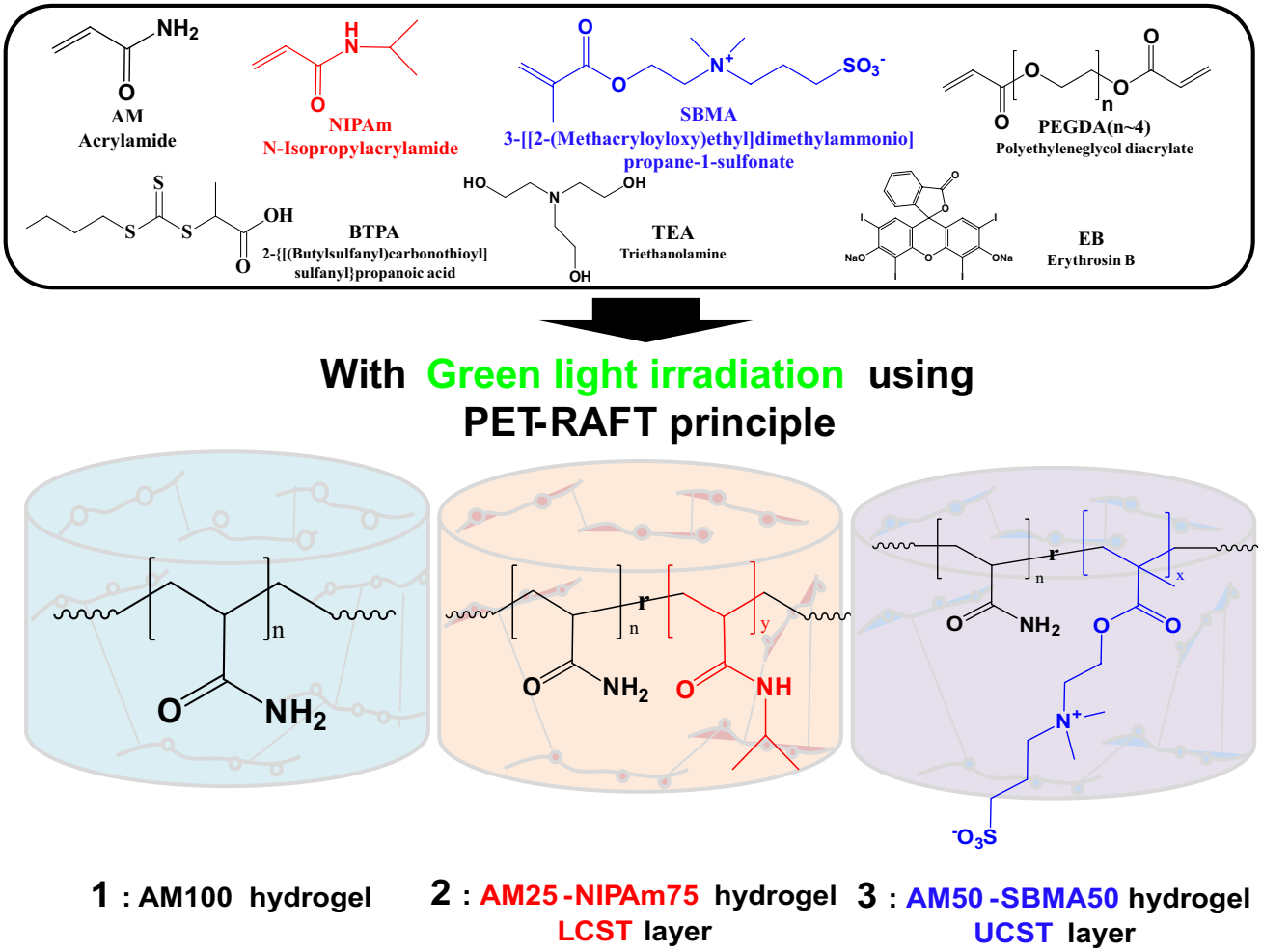

SCHEME 1 | Preparation of hydrogels by PET-RAFT polymerization with visible light (green light, 518 nm).

2.3.2 | Frequency Sweep Analysis of Rheological Properties

Modulus measurements with a rheometer were performed for the hydrogel samples of cylindrical shapes with 11 mm diameter and thickness (2 and 4.5 mm) after PET-RAFT polymerization and orthogonal reaction. For analysis of the modulus, a rheometer with a frequency sweep method was used with Physica MCR 101 (Anton Paar, Austria), set at 10% shear strain and 5000.1 rad s^{-1} angular frequency. The dynamic storage and loss modulus were measured at a temperature of 4°C and 70°C.

2.3.3 | Swelling Ratio Analysis

Swelling ratio of the hydrogels was measured. The weight of the samples was measured, then immersed in water. The change of the swollen hydrogels weight was measured on a timely basis. The swelling ratio of the hydrogel was calculated as follows:

$$\text{Swelling Ratio} = \frac{(\text{Measured weight of sample in the swelling state})(\text{g})}{(\text{Reference sample weight})(\text{g})} \quad (1)$$

The swelling ratios of the hydrogels were measured at the different temperatures (4°C and 70°C).

2.3.4 | Young's Modulus Measurement

The Yong's modulus of the gels was measured with a digital pressure regulator (SMC ITV 2030). The deformation of the gels was captured with a camera (Canon Inc). The images were processed by MATLAB R2019b Single Camera Calibration App.

3 | Results and Discussion

3.1 | Preparation of Hydrogel by PET-RAFT Polymerization

The ATR FT-IR spectra were measured to evaluate the polymerization progress for the hydrogels (Figure 2). In the ATR FT-IR spectra of **1**, **2**, and **3** inks, peaks at 1582, 1614, and 1602 cm^{-1} corresponded to CH_2 bending of vinyl groups. After irradiation with green light on the inks, these peak intensities of the hydrogels diminished compared with those of their inks. The ATR FT-IR spectrum of hydrogel **2** showed a peak for N—H bending of polyacrylamide at a wavenumber of 1625 cm^{-1}, which was not observed in that of the **2** monomer mixture. Additionally, the spectrum of the **2** monomer mixture and hydrogel contained specific double peaks at wavenumbers of 1370 and 1388 cm^{-1}, corresponding to C—H stretching of isopropyl groups. The ATR FT-IR spectrum of the 3 ink and hydrogel contained peaks at wavenumbers of 1040 and 1173 cm^{-1}, which corresponded to S═O stretching of the sulfobetaine moiety [42, 43].

The ATR FT-IR spectra of the hydrogels suggested successful PET-RAFT polymerization of the parent inks with green light irradiation. Through PET-RAFT polymerization, the chemical structures such as isopropyl groups and ionic structures (ammonium and sulfonic groups) were well maintained in the hydrogels of **2** and **3**.

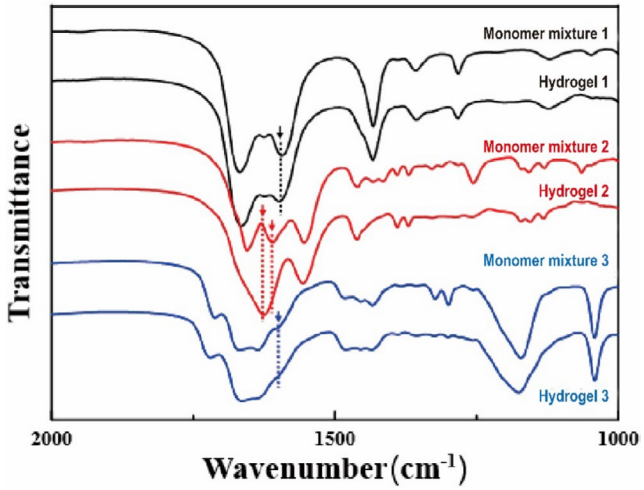

FIGURE 2 | FTIR spectra of the monomer mixtures and hydrogels (**1**: Black, **2**: Red, and **3**:Blue).

3.2 | Rheology of Hydrogels at Different Temperature

The viscoelastic properties of the hydrogels were investigated by dynamic mechanical analysis using a rheometer with a frequency sweep method at different temperatures (Figure 3 and Figures S3–S5). In all the hydrogels, storage (G') and loss (G'') modulus increased with increasing angular frequency. For the 1 hydrogel, the storage modulus at 4°C and 70°C was almost the same. However, the slope of the storage modulus from high frequency to low frequency was slightly lower at 4°C compared to that at 70°C. On the other hand, the 1 hydrogel showed significantly higher loss modulus at 70°C than that at 4°C. This indicated that the 1 hydrogel, which was composed of AM, had higher viscoelastic properties at higher temperatures.

In the case of hydrogel **2**, the storage modulus also showed similar values and trends at 4°C and 70°C. Interestingly, the loss (G'') modulus for hydrogel **2** was higher than the storage (G') modulus at 70°C, which was totally different from the behavior observed in hydrogel **1**. It was suggested that hydrogel **2** would exhibit higher energy loss at 70°C. This can be explained by the LCST of hydrogel **2**. At elevated temperatures (70°C), the molecular structure of the PolyNIPAm units aggregated into clusters, leading to higher hydrophobicity. Consequently, molecular-scale phase separation occurred between PolyNIPAm and water in the hydrogel **2** sample. This caused the loss modulus to be higher than the storage modulus under 70°C conditions, due to an increase in liquid-like properties [40, 44, 45].

The hydrogel **3** showed lower storage and loss modulus than those of hydrogels **1** and **2**. At 70°C, the storage (G') and loss modulus (G'') of hydrogel **3** increased by 10 times compared to those at 4°C. This significantly higher modulus at higher temperatures can be attributed to the ionic functional groups

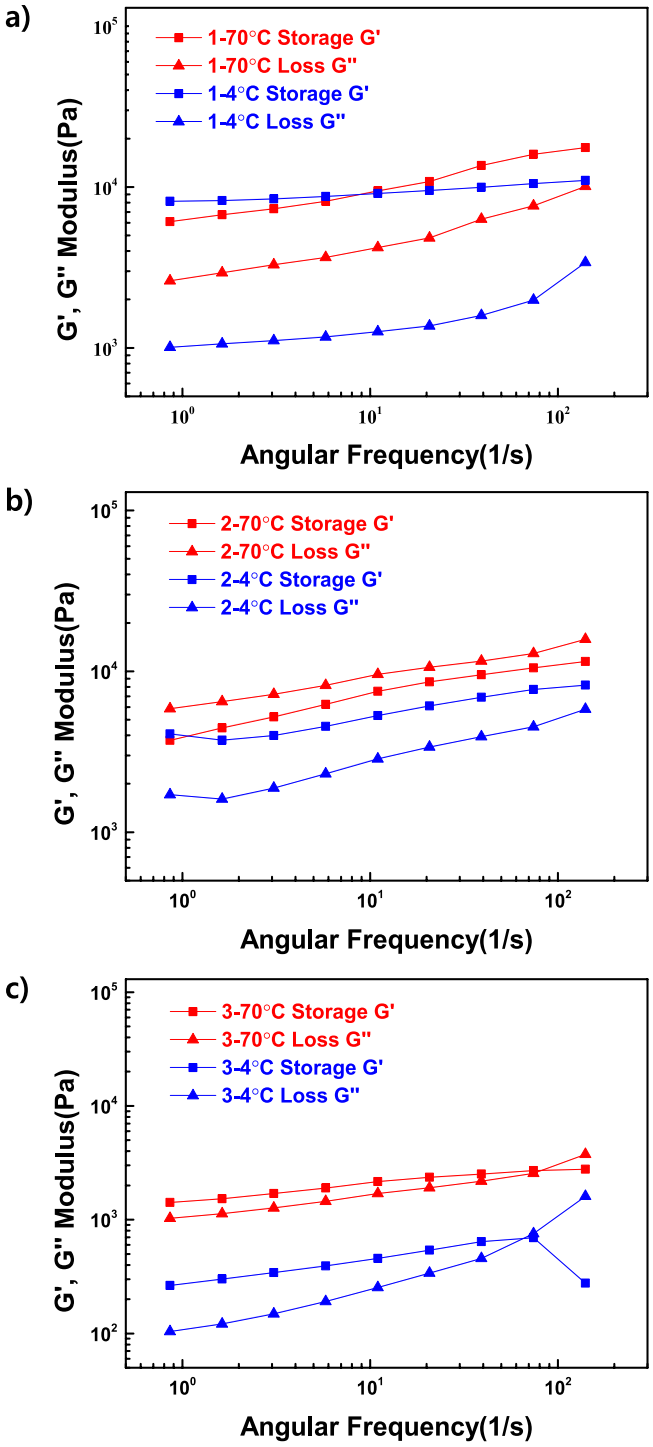

FIGURE 3 | Frequency sweep analysis for the storage modulus and loss modulus of the hydrogels. (a) **1** (AM100), (b) **2** (AM25-NIPAM75), and (c) **3** (AM50-SBMA50).

in hydrogel **3**, which contain sulfobetaine units. These ionic groups interacted more strongly with each other at higher temperatures (70°C) compared to lower temperatures (4°C). Overall, a series of hydrogels that showed thermoresponsive rheology were successfully obtained through PET-RAFT polymerization.

All of the samples' Young's modulus trends were almost similar to their storage modulus trends. The Young's modulus

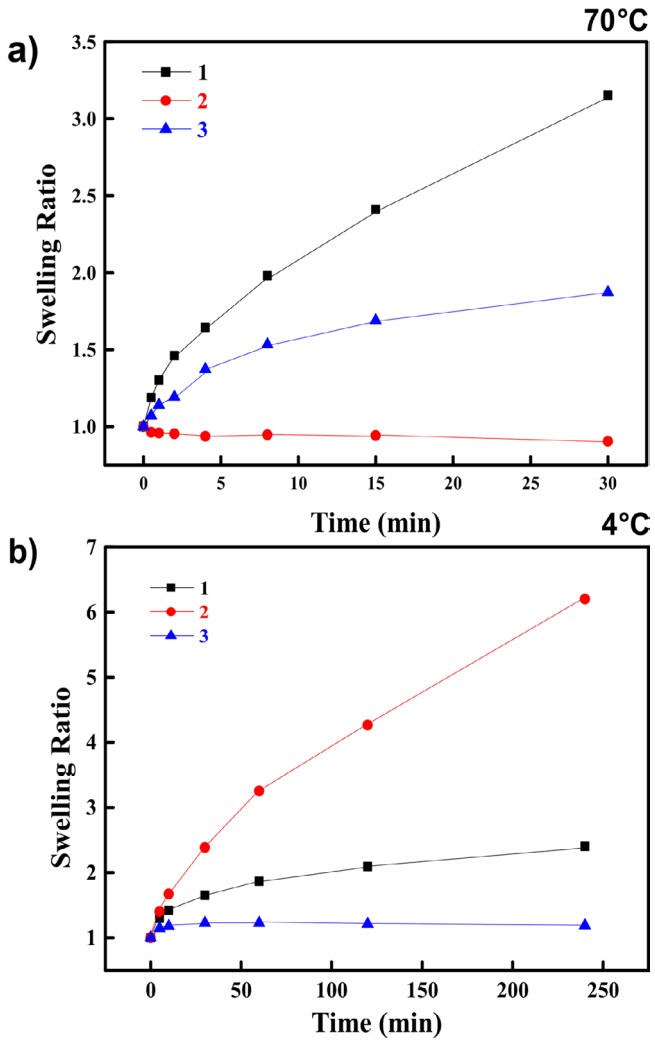

FIGURE 4 | Time-course of swelling ratios of the hydrogels at (a) 70°C and (b) 4°C.

graph with calculation can be referenced in the Supporting Information at the F series sections.

3.3 | Swelling Properties of Hydrogels at Different Temperature

The swelling ratio of the hydrogels was evaluated at different temperatures (4°C and 70°C) in water (Figure 4). For all the hydrogels, the swelling ratio increased with increasing time. At 70°C, hydrogels **1**, **2**, and **3** showed swelling ratios of 3.15, 0.90, and 1.87, respectively (at 30 min, Table S1). The highest swelling ratio at 70°C was observed for hydrogel **1** (AM100). On the other hand, at 4°C, the swelling ratios of hydrogels **1**, **2**, and **3** reached 2.40, 6.20, and 1.18, respectively (at 240 min, Table S1b). The swelling behaviors drastically changed at the lower temperature (4°C), where the swelling ratio of hydrogel **2** was the highest. The thermoresponsive properties of the hydrogels were highlighted in their swelling ratio in water. Hydrogel **2** (AM25-NIPAM75), with LCST, exhibited the lowest swelling ratio (0.90) at 70°C, while the highest swelling ratio (6.20) was obtained at 4°C. Conversely, for hydrogel **3** (AM50-SBMA50), which has UCST, a contrasting trend in the swelling ratio was

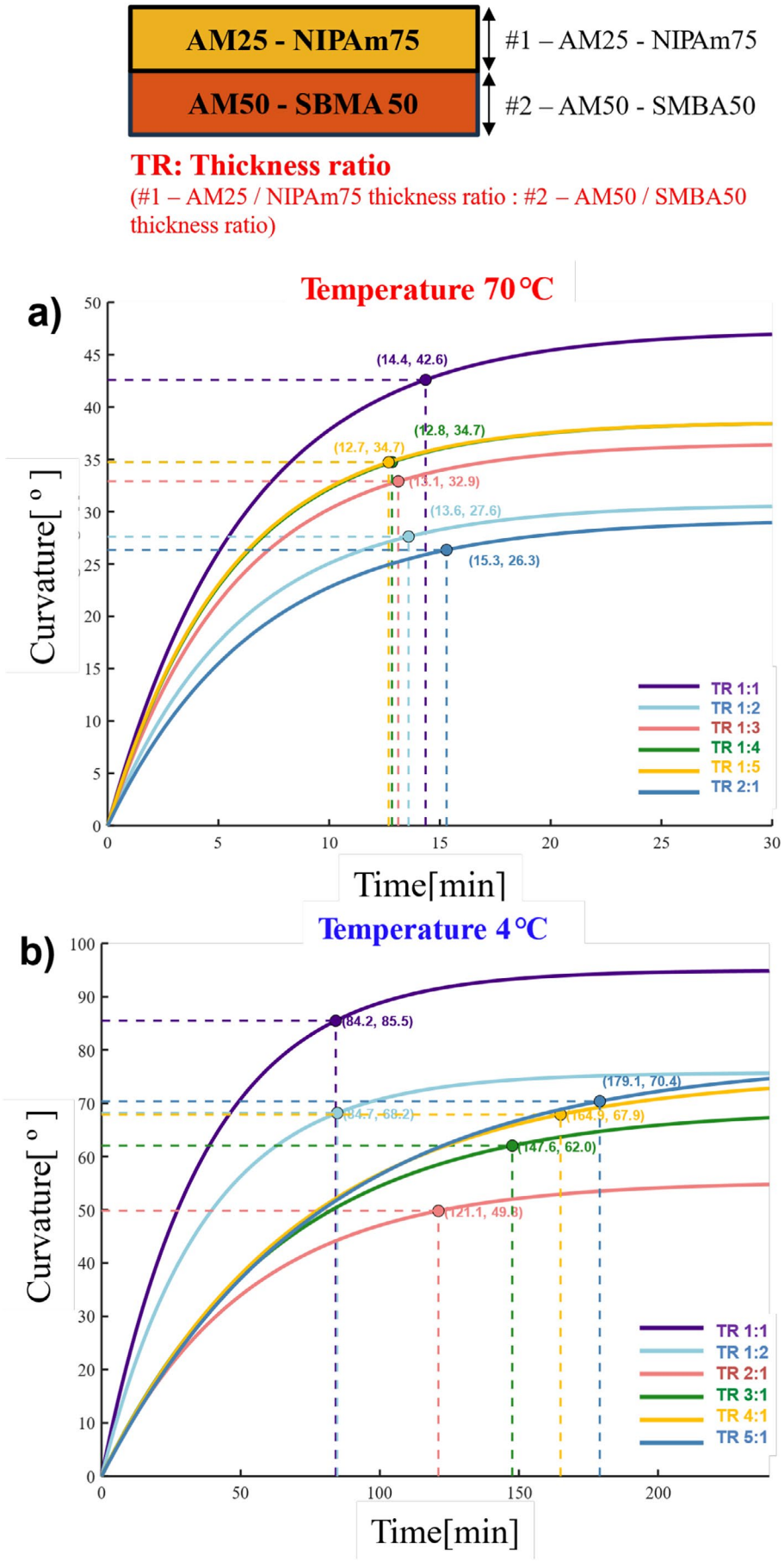

FIGURE 5 | Legend on next page.

FIGURE 5 | Simulated time-course of curvature of **2**/**3** bilayer hydrogels (1st layer = **2**, 2nd layer = **3**) with different thickness ratio (TR) ((a) 70°C and (b) 4°C). The plots highlight specific time when curvature reached 90% of its maximum.

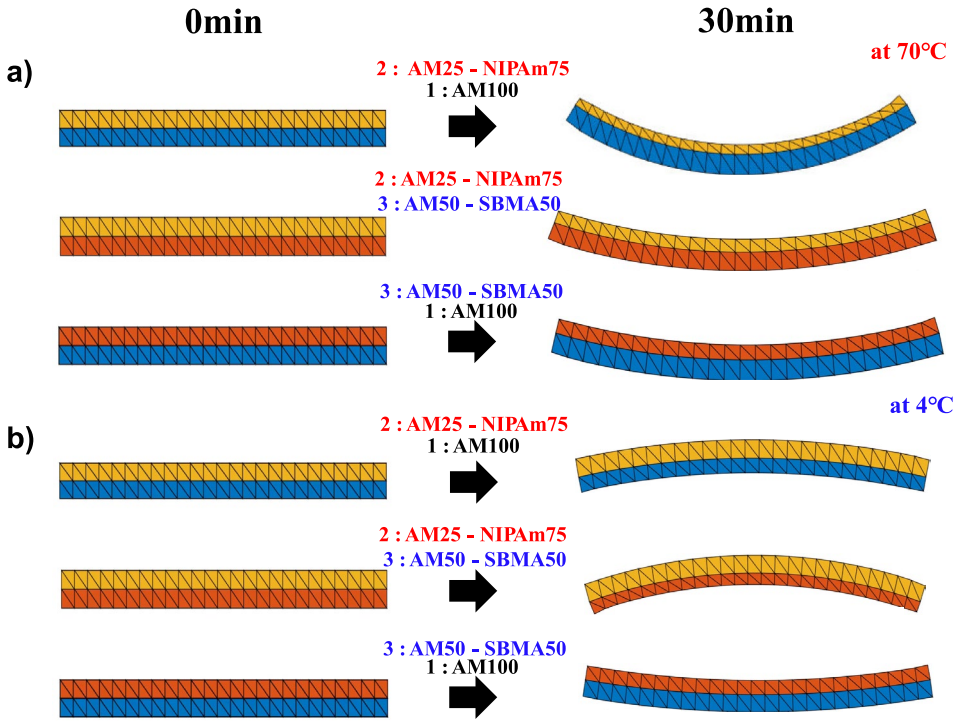

FIGURE 6 | Computer simulation of hydrogel curvature by swelling in water at (a) 70°C and (b) 4°C.

obtained. The combination of these thermoresponsive hydrogels would provide rapid and dramatic 4D motions via temperature changes, enabling various mechanical responses and functional properties under different conditions.

3.4 | Design of Bilayer Hydrogels for 4D Motions via Temperature Changes Based on Computer Simulations

To realize 4D materials, bilayers composed of thermoresponsive hydrogels were designed. The 1st and 2nd layers were composed of hydrogels **2** (AM25-NIPAm75) and **3** (AM50-SMBA50), respectively. Length and total thickness of the bilayers were fixed at 25 and 4 mm, respectively. A thickness ratio (TR) was defined as the ratio of the thickness of hydrogel **2** to that of hydrogel **3**. Upon temperature changes in water, the bending curvature was predicted by computer simulations using an open-source simulator (SFEM-4DP). The simulator was based on finite element analysis, and material properties such as Young's modulus, density, Poisson's ratio, and swelling ratio were input parameters (Figures S6–S8). The simulation provided the time course of the curvature, demonstrating that the bilayer structure with a TR of 1:1 achieved the highest curvature at both temperatures (Figure 5) (70°C and 4°C). Through screening the TR based on the computer simulations, drastic 4D motions were successfully estimated (Supporting Information).

The 4D motions of the bilayers were further simulated from the swelling ratio of various hydrogel combinations. To realize various curvature patterns and angles, a series of combinations of hydrogels **1**, **2**, and **3** in the bilayer design was examined. The TR was fixed at 1:1, and each layer had the same dimensions ($25 \times 5 \times 2\,mm^3$). At 70°C, all the bilayers showed a downward curvature within 30 min by swelling in water (Figure 6a). Interestingly, lowering the temperature (to 4°C) induced an upward curvature of bilayers with **2/1** and **2/3** hydrogels (Figure 6b), which were inverse *curvatures* to those at 70°C. It was suggested that the combination patterns of the thermoresponsive hydrogels were important to control the curvature directions and angles.

All of the simulation source data is contained in the Supporting Information data of simulations for this paper.

3.5 | 4D Motions of Bilayers Composed of Thermo-Responsive Hydrogels

Finally, we prepared bilayer hydrogels for 4D motions upon temperature changing based on the computer simulation. The swelling of the hydrogel bilayers in water was observed during a temperature swing from 4°C to 70°C (Figure 7). The **2/3** and **2/1** bilayer hydrogels were evaluated for their 4D motions against the temperature swing as expected in the computer simulation, which are shown in Figure 7a,b, respectively.

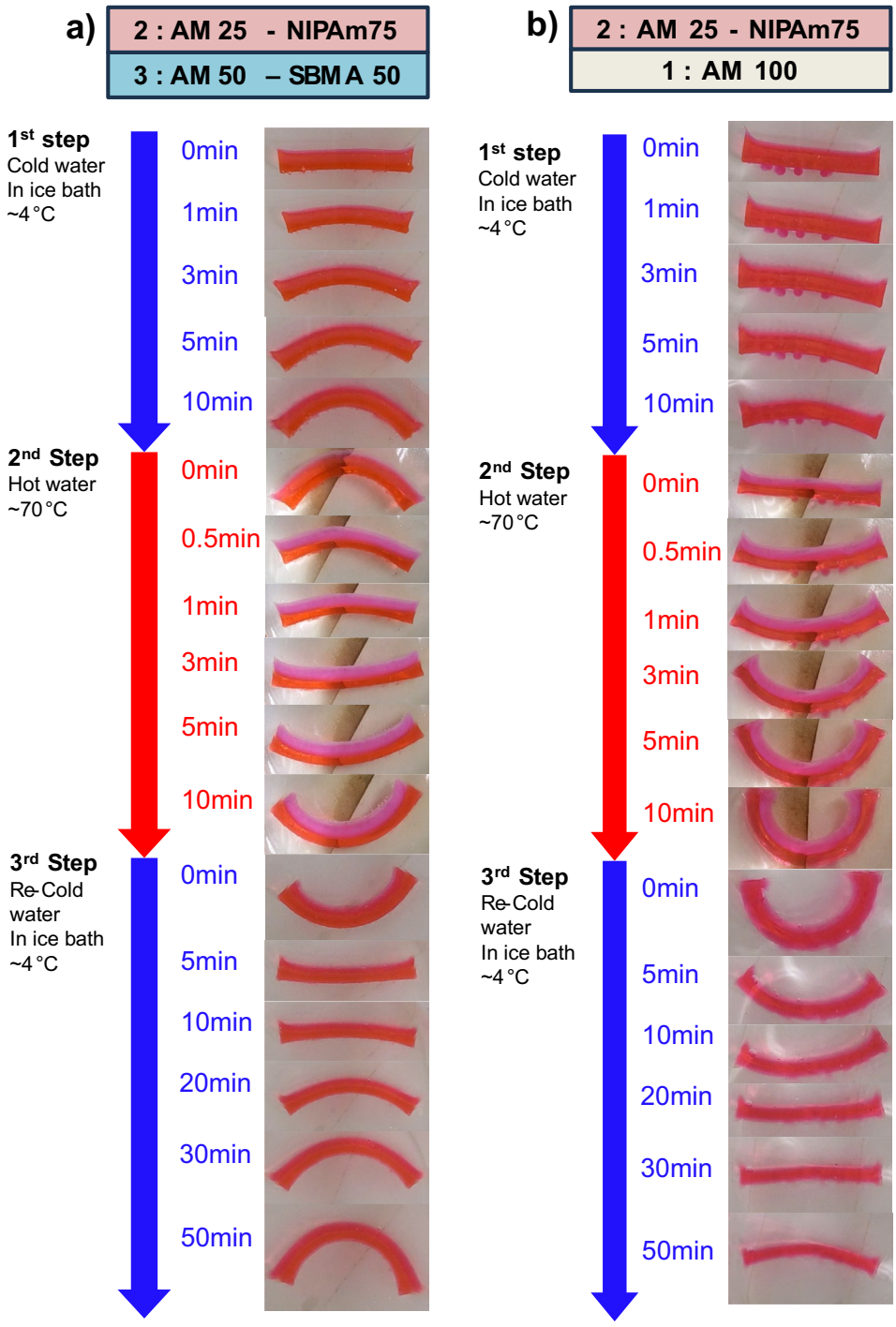

FIGURE 7 | 4D motions of the bilayer hydrogels with (a) **2/3** and (b) **2/1** at temperature swings. 1st step = 4°C for 10 min, 2nd step = 70°C for 10 min, 3rd step = 4°C for 50 min.

In the case of the **2/3** bilayer hydrogel, in the first step at 4°C, the **2/3** bilayer hydrogel moved upward, and the curvature angle changed from 0.0° to +54.8° (+54.8° change) (Figure 7a, top). In the second step at 70°C, the hydrogel moved in the inverse direction from +54.8° to −76.6° (−131.4° change), and the movement occurred within 10 min (Figure 7a, middle). In the third step at 4°C again, the hydrogel moved upward from −76.6° to +78.8° (+155.4° change) (Figure 7a, bottom). In the case of the **2/1** bilayer hydrogel, in the first step at 4°C, the hydrogel moved upward from 0.0° to +26.0° (+26.0° change) (Figure 7b, top). In the second step at 70°C, the hydrogel moved in the inverse direction from +26.0° to −98.4° (−124.4° change) (Figure 7b, middle). In the third step at 4°C again, the hydrogel moved upward from −98.4° to +21.2° (+119.6° change) (Figure 7b, bottom). Compared with the computer simulations, the observed 4D motions of the bilayer hydrogels well matched the simulated 4D motions (Figure 6).

Successfully, the 4D motions of the bilayer hydrogels were realized by utilizing the reversible swelling in water upon temperature changes. By incorporating thermoresponsive hydrogels with LCST and UCST characteristics, the 4D motions could be designed by

their swelling properties and their combination for bilayer structures, which were well predicted by computer simulations.

4 | Conclusions

A strategy for controlling the 4D motions of thermoresponsive hydrogels was developed. The hydrogels with LCST and UCST were synthesized by PET-RAFT polymerization, and they showed drastic changes in their viscoelastic properties and swelling behaviors upon temperature changes. These physical properties of the hydrogels enabled us to design 4D materials by combining different types of hydrogels for bilayer structures. The computer simulations predicted 4D motions, demonstrating that various curvatures and bending angles of the bilayer hydrogels could be achieved by tuning the TR and combination patterns. Our study provided valuable insights into the rheological properties of these hydrogels and emphasized computer simulations as a critical tool for 4D materials. Merging these techniques with 3D printing would broaden the scope of 4D materials with high complexity and tunability for potential applications in cutting-edge fields such as robotics, aerospace, and medical technologies.

Acknowledgments

This article is based on results obtained from a project, JPNP14004, commissioned by the New Energy and Industrial Technology Development Organization (NEDO).

Data Availability Statement

The authors confirm that the data supporting the findings of this study are available within the article and its Supporting Information.

References

1. X. Wang, G. Mao, J. Ge, et al., "Untethered and Ultrafast Soft-Bodied Robots," *Communications Materials* 1 (2020): 1–10, https://doi.org/10.1038/s43246-020-00067-1.

2. D. Rus and M. Tolley, "Design, Fabrication and Control of Soft Robots," *Nature* 521 (2015): 467–475, https://doi.org/10.1038/nature14543.

3. B. Maheswari, P. E. Jangadeesh Babu, and M. Agarwal, "Role of *N*-Vinyl-2-Pyrrolidinone on the Thermoresponsive Behavior of PNIPAm Hydrogel and Its Release Kinetics Using Dye and Vitamin-B12 as Model Drug," *Journal of Biomaterials Science, Polymer Edition* 25 (2013): 269–286, https://doi.org/10.1080/09205063.2013.854149.

4. Y. Yuan, K. Raheja, N. B. Milbrandt, et al., "Thermoresponsive Polymers With LCST Transition: Synthesis, Characterization, and Their Impact on Biomedical Frontiers," *RSC Applied Polymers* 1 (2023): 158–189, https://doi.org/10.1039/D3LP00114H.

5. H. Asai, M. Shibata, M. Takenaka, et al., "Micelle-Crosslinked Hydrogels With Stretchable, Self-Healing, and Selectively Adhesive Properties: Random Copolymers Work as Dynamic Yet Self-Sorting Domains," *Aggregate* 4 (2023): 1–13, https://doi.org/10.1002/agt2.316.

6. E. P. Dam, H. Yuan, P. H. J. Kouwer, and H. J. Bakker, "Structure and Dynamics of a Temperature-Sensitive Hydrogel," *Journal of Physical Chemistry. B* 125 (2021): 8219–8224, https://pubs.acs.org/doi/10.1021/acs.jpcb.1c03121.

7. Y. Li, W. Zheng, B. Li, J. Dong, G. Gao, and Z. Jiang, "Double-Layer Temperature-Sensitive Hydrogel Fabricated by 4D Printing With Fast Shape Deformation," *Colloids and Surfaces A: Physicochemical and Engineering Aspects* 648 (2022): 129307, https://doi.org/10.1016/j.colsurfa.2022.129307.

8. H. Zuo, Y. Yang, D. Zheng, et al., "Mussel-Inspired Hydrogels With UCST for Temperature-Controlled Reversible Adhesion," *Giant* 16 (2023): 100182, https://doi.org/10.1016/j.giant.2023.100182.

9. M. Lehmann, P. Krause, V. Miruchna, and R. Klitzing, "Tailoring PNIPAM Hydrogels for Large Temperature-Triggered Changes in Mechanical Properties," *Colloid and Polymer Science* 297 (2019): 633–640, https://doi.org/10.1007/s00396-019-04470-0.

10. V. S. Raghuwanshi, D. J. Mendoza, C. Browne, et al., "Effect of Temperature on the Conformation and Functionality of Poly(N-Isopropylacrylamide) (PNIPAM)-grafted Nanocellulose Hydrogels," *Journal of Colloid and Interface Science* 652 (2023): 1609–1619, https://doi.org/10.1016/j.jcis.2023.08.152.

11. N. A. Shaibie, N. A. Ramli, N. D. F. M. Faizal, T. Srichana, and M. C. I. M. Amin, "Poly(*N*-Isopropylacrylamide)-Based Polymers: Recent Overview for the Development of Temperature-Responsive Drug Delivery and Biomedical Applications," *Macromolecular Chemistry and Physics* 224 (2023): 2300157, https://doi.org/10.1002/macp.202300157.

12. Z. H. Ghauri, A. Islam, M. A. Qadir, et al., "Development and Evaluation of pH-Sensitive Biodegradable Ternary Blended Hydrogel Films (Chitosan/Guar Gum/PVP) for Drug Delivery Application," *Scientific Reports* 11 (2021): 21255, https://doi.org/10.1038/s41598-021-00452-x.

13. R. Marcombe, S. Cai, W. Hong, X. Zhao, Y. Lapusta, and Z. Suo, "A Theory of Constrained Swelling of a pH-Sensitive Hydrogel," *Soft Matter* 6 (2010): 784, https://doi.org/10.1039/B917211D.

14. Y. Xing, B. Zeng, and W. Yang, "Light Responsive Hydrogels for Controlled Drug Delivery," *Frontiers in Bioengineering and Biotechnology* 10 (2022): 1–9, https://doi.org/10.3389/fbioe.2022.1075670.

15. J. Chen, J. Huang, H. Zhang, and Y. Hu, "A Photoresponsive Hydrogel With Enhanced Photoefficiency and the Decoupled Process of Light Activation and Shape Changing for Precise Geometric Control," *ACS Applied Materials & Interfaces* 12 (2020): 38647–38654, https://doi.org/10.1021/acsami.0c09475.

16. N. P. Murphy and K. J. Lampe, "Mimicking Biological Phenomena in Hydrogel-Based Biomaterials to Promote Dynamic Cellular Responses," *Journal of Physical Chemistry. B* 3 (2015): 7867–7880, https://doi.org/10.1039/C5TB01045D.

17. H. Yang, M. Ji, M. Yang, et al., "Fabricating Hydrogels to Mimic Biological Tissues of Complex Shapes and High Fatigue Resistance," *Matter* 4 (2021): 1935–1946, https://doi.org/10.1016/j.matt.2021.03.010.

18. M. Najafi, M. Habibi, R. Fokkink, W. E. Hennink, and T. Vermonden, "LCST Polymers With UCST Behavior," *Soft Matter* 17 (2021): 2132–2141, https://doi.org/10.1039/D0SM01505A.

19. H. Sun, J. Chen, X. Han, and H. Liu, "Multi-Responsive Hydrogels With UCST- and LCST-Induced Shrinking and Controlled Release Behaviors of Rhodamine B," *Materials Science and Engineering: C* 82 (2018): 284–290, https://doi.org/10.1016/j.msec.2017.08.067.

20. L. Tang, L. Wang, X. Yang, Y. Feng, Y. Li, and W. Feng, "Poly(*N*-Isopropylacrylamide)-based Smart Hydrogels: Design, Properties and Applications," *Progress in Materials Science* 115 (2021): 100702, https://doi.org/10.1016/j.pmatsci.2020.100702.

21. C. Echeverria, D. Lopez, and C. Mijangos, "UCST Responsive Microgels of Poly(Acrylamide-Acrylic Acid) Copolymers: Structure and Viscoelastic Properties," *Macromolecules* 42 (2009): 9118–9123, https://doi.org/10.1021/ma901316k.

22. Y. Nan, C. Zhao, G. Beaudoin, and X. X. Zhu, "Synergistic Approaches in the Design and Applications of UCST Polymers," *Macromolecular Rapid Communications* 44 (2023): 2300261, https://doi.org/10.1002/marc.202300261.

23. J. Wang, Y. Wu, K. Zhao, et al., "Mechanically Robust, Time-Programmable, Janus Hydrogel Actuator, and the Insights Into Its

Driving Principles," *ACS Applied Polymer Materials* 7 (2025): 3670–3685, https://doi.org/10.1021/acsapm.4c03888.

24. L. Hua, M. Xie, Y. Jian, B. Wu, C. Chen, and C. Zhao, "Multiple-Responsive and Amphibious Hydrogel Actuator Based on Asymmetric UCST-Type Volume Phase Transition," *ACS Applied Materials & Interfaces* 11 (2019): 43641–43648, https://doi.org/10.1021/acsami.9b17159.

25. J. Zheng, P. Xiao, X. Le, et al., "Mimosa Inspired Bilayer Hydrogel Actuator Functioning in Multi-Environments," *Journal of Materials Chemistry C* 6 (2018): 1320–1327, https://doi.org/10.1039/C7TC04879C.

26. A. Clancy, D. Chen, J. Bruns, et al., "Hydrogel-Based Microfluidic Device With Multiplexed 3D In Vitro Cell Culture," *Scientific Reports* 12 (2022): 17781, https://doi.org/10.1038/s41598-022-22439-y.

27. S. Yang, S. Sarkar, X. Xie, D. Li, and J. Chen, "Application of Optical Hydrogels in Environmental Sensing," *Energy & Environmental Materials* 7 (2024): e12646, https://doi.org/10.1002/eem2.12646.

28. X. Du, J. Zhai, X. Li, Y. Zhang, N. Li, and X. Xie, "Hydrogel-Based Optical Ion Sensors: Principles and Challenges for Point-of-Care Testing and Environmental Monitoring," *ACS Sensors* 6 (2021): 1990–2001, https://doi.org/10.1021/acssensors.1c00756.

29. M. Boustta, P. E. Colombo, S. Lenglet, S. Poujol, and M. Vert, "Versatile UCST-Based Thermoresponsive Hydrogels for Loco-Regional Sustained Drug Delivery," *Journal of Controlled Release* 174 (2014): 1–6, https://doi.org/10.1016/j.jconrel.2013.10.040.

30. L. Liu, M. Gao, X. Fan, Z. Lu, and Y. Li, "Fast Fabrication of Stimuli-Responsive MXene-Based Hydrogels for High-Performance Actuators With Simultaneous Actuation and Self-Sensing Capability," *Journal of Colloid and Interface Science* 684 (2025): 469–480, https://doi.org/10.1016/j.jcis.2025.01.032.

31. L. Liu, Y. Li, Z. Lu, R. Miao, and N. Zhang, "Thermal and Light-Driven Soft Actuators Based on a Conductive Polypyrrole Nanofibers Integrated Poly(N-Isopropylacrylamide) Hydrogel With Intelligent Response," *Journal of Colloid and Interface Science* 675 (2024): 336–346, https://doi.org/10.1016/j.jcis.2024.07.017.

32. C. Qian, Y. Li, L. Liu, C. Chen, and L. Han, "NIR Responsive and Conductive PNIPAM/PANI Nanocomposite Hydrogels With High Stretchability for Self-Sensing Actuators," *Journal of Materials Chemistry C* 20, no. 20 (2023): 2201303, https://doi.org/10.1039/D3TC00990D.

33. C. Qian, Y. Li, C. Chen, et al., "A Stretchable and Conductive Design Based on Multi-Responsive Hydrogel for Self-Sensing Actuators," *Journal of Chemical Engineering* 454 (2023): 140263, https://doi.org/10.1016/j.cej.2022.140263.

34. J. Li, Q. Ma, Y. Xu, et al., "Highly Bidirectional Bendable Actuator Engineered by LCST–UCST Bilayer Hydrogel With Enhanced Interface," *ACS Applied Materials Interfaces* 12 (2020): 55290–55298, https://doi.org/10.1021/acsami.0c17085.

35. F. Puza and K. Lienkamp, "3D Printing of Polymer Hydrogels—From Basic Techniques to Programmable Actuation," *Advanced Functional Materials* 32 (2022): 2205345, https://doi.org/10.1002/adfm.202205345.

36. K. Benyahia, H. Serket, R. Prod'hon, et al., "A Computational Design Approach for Multi-Material 4D Printing Based on Interlocking Blocks Assembly," *Additive Manufacturing* 58 (2022): 102993, https://doi.org/10.1016/j.addma.2022.102993.

37. T. Kopac, "Mathematical Model for Characterization of Temperature-Responsive Polymers: A Study on the Rheological Behavior of Gelatin and Poly (*N*-Isopropylacrylamide)," *Polymer Testing* 133 (2024): 108402, https://doi.org/10.1016/j.polymertesting.2024.108402.

38. X. Shi, J. Zhang, N. Corrigan, and C. Boyer, "PET-RAFT Facilitated 3D Printable Resins With Multifunctional RAFT Agents," *Materials Chemistry Frontiers* 5 (2021): 2271–2282, https://doi.org/10.1039/D0QM00961J.

39. Z. Zhang, N. Corrigan, A. Bagheri, J. Jin, and C. Boyer, "A Versatile 3D and 4D Printing System Through Photocontrolled RAFT Polymerization," *Angewandte Chemie, International Edition* 58 (2019): 17954–17963, https://doi.org/10.1002/anie.201912608.

40. A. Das, A. Babu, s. Chakraborty, J. F. R. Van Guyse, R. Hoogenboom, and S. Maji, "Poly(*N*-Isopropylacrylamide) and Its Copolymers: A Review on Recent Advances in the Areas of Sensing and Biosensing," *Advanced Functional Materials* 34 (2024): 2402432, https://doi.org/10.1002/adfm.202402432.

41. C. Jee, H. Matsumoto, T. Horiuchi, et al., "Preparation of 4D Hydrogels With PET-RAFT and Orthogonal Photo-Reactions," *RSC Applied Polymers* 3, no. 1 (2025): 156–162, https://doi.org/10.1039/d4lp00232f.

42. T. Munk, S. Baldursdottir, S. Heitala, et al., "Investigation of the Phase Separation of PNIPAM Using Infrared Spectroscopy Together With Multivariate Data Analysis," *Polymer* 54 (2013): 6947–6953, https://doi.org/10.1016/j.polymer.2013.10.033.

43. M. M. Leitao, C. G. Alves, D. Melo-Diogo, R. Lima-Sousa, A. F. Moreira, and I. J. Correia, "Sulfobetaine Methacrylate-Functionalized Graphene Oxide-IR780 Nanohybrids Aimed at Improving Breast Cancer Phototherapy," *RSC Advances* 10 (2020): 38621, https://doi.org/10.1039/D0RA07508F.

44. M. Radecki, J. Spěváček, A. Zhigunov, Z. Sedláková, and L. Hanyková, "Temperature-Induced Phase Transition in Hydrogels of Interpenetrating Networks of Poly(*N*-Isopropylacrylamide) and Polyacrylamide," *European Polymer Journal* 68 (2015): 68–79, https://doi.org/10.1016/j.eurpolymj.2015.04.019.

45. S. Lanzalaco, J. Mingot, J. Torras, C. Alemán, and E. Armelin, "Recent Advances in Poly(N-Isopropylacrylamide) Hydrogels and Derivatives as Promising Materials for Biomedical and Engineering Emerging Applications," *Advanced Engineering Materials* 25 (2023): 2201303, https://doi.org/10.1002/adem.202201303.

Supporting Information

Additional supporting information can be found online in the Supporting Information section.